

Dynamics of the two-dimensional axial third-nearest-neighbor Ising model: Entrainment and diffusivity

G. N. Hassold, J. F. Dreitlein, P. D. Beale, and J. F. Scott
 Department of Physics, University of Colorado, Boulder, Colorado 80309
 (Received 1 November 1985)

We report results of a Monte Carlo study of the "equilibrium dynamics" of the two-dimensional axial third-nearest-neighbor Ising model, which exhibits a modulated phase incommensurate with the lattice spacing. The linear response function is shown to be a good predictor of model phases and boundaries. Two phenomenological observations, entrainment and diffusivity, are related to other studies, both theoretical and experimental.

Models with competing interactions have been of interest because they yield a rich structure of modulated phases.¹ Many techniques have been used to study the phase diagrams of models of this type. They include free-fermion analysis,² domain-wall free-energy calculations,³ exact solutions of equivalent quantum Hamiltonian models,⁴ phenomenological finite-size scaling analysis,⁵ series analysis,⁶ and Monte Carlo simulations.⁷ In particular, the three-dimensional axial third-nearest-neighbor Ising (A3NNI)^{8,9} model has been shown to have an apparent correspondence with a number of crystals. Most of the Monte Carlo simulations to date have examined the static equilibrium properties of such models. The static structure factor has been examined to determine the location of the commensurate-incommensurate phase transition boundaries. Here we report on a dynamical equilibrium simulation of the two-

dimensional A3NNI model, which demonstrates the usefulness of another predictor of the commensurate-incommensurate transition: the linear response function.

A phase diagram of the A3NNI model (Fig. 1) was obtained by a conventional Monte Carlo study, using the Hamiltonian

$$\mathcal{H} = \sum_{i,j} \left(-\frac{1}{2} \right) (J_0 S_{i,j} S_{i \pm 1, j} + J_1 S_{i,j} S_{i,j \pm 1} + J_2 S_{i,j} S_{i,j \pm 2} + J_3 S_{i,j} S_{i,j \pm 3}) , \quad (1)$$

where $J_0 = +1$, $J_1 = -1$, $0 \geq J_2 \geq -1$, $J_3 = \pm 0.1$, and i and j denote Cartesian coordinates on a square lattice. The three commensurate phases shown have the following structure:

$$\langle 1 \rangle \dots \downarrow \uparrow \downarrow \uparrow \downarrow \uparrow \dots, \quad \langle 1, 2 \rangle \dots \downarrow \uparrow \downarrow \uparrow \downarrow \uparrow \downarrow \uparrow \dots, \quad \langle 2 \rangle \dots \downarrow \downarrow \uparrow \uparrow \downarrow \downarrow \uparrow \uparrow \dots$$

The peak in the static structure factor

$$S(k) = \sum_r \exp(-ikr) \left[\sum_x [M(x+r)M(x)] - \sum_x [M(x+r)] \sum_x [M(x)] \right] \quad (2)$$

[where $M(x)$ is the magnetization of row x] gives the clearest signal of the phase transitions: In the commensurate (C) phase it was narrow but very weak, in the incommensurate (IC) phase it was narrow and intense, and in the "paramagnetic" (PM) phase it was broad and weak. This is consistent with other work on the structure factor in modulated systems.⁵ The peak in $S(k)$ occurs at a k value equal to the modulation wave vector. As the temperature was swept, the value of the temperature at half-maximum intensity of $S(k)$ was taken as the transition point. Hysteresis between warming and cooling runs established the error bars.

In order to exploit the vector capabilities of the Control Data Corporation CYBER 205 (which was used to run the simulations), a "four-color parquette" updating scheme was used in which groups of spins which do not interact directly were updated together (Fig. 2). This is a generalization of the "two-color checkerboard" technique used to vectorize models with nearest-neighbor interactions.¹⁰ Thus, in the figure all the sites labeled A would be updated together,

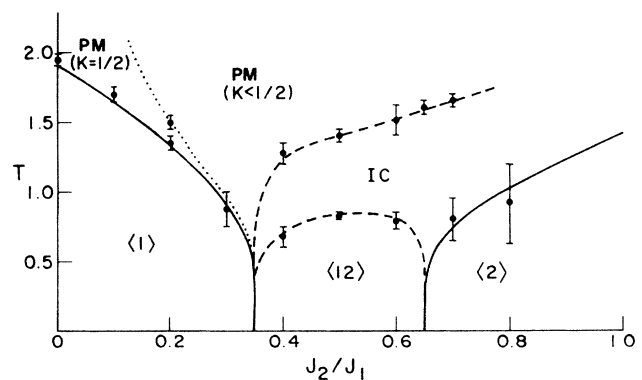


FIG. 1. Phase diagram of the 2D A3NNI model. $\langle 1 \rangle$, $\langle 12 \rangle$, and $\langle 3 \rangle$ are commensurate phases. All lines are continuous transitions. Solid lines are domain-wall free-energy calculations;^{3,14} dashed lines are to guide the eye. The dotted line is the disorder line (not a true phase transition).

D	A	B	C	D	A	B	C
C	D	A	B	C	D	A	B
B	C	D	A	B	C	D	A
A	B	C	D	A	B	C	D
D	A	B	C	D	A	B	C
C	D	A	B	C	D	A	B
B	C	D	A	B	C	D	A
A	B	C	D	A	B	C	D

FIG. 2. Updating scheme (shown for an 8x8 lattice).

then those labeled *B*, and so on, until the entire lattice had been passed over (the subscripts indicate the numbering scheme used for the lattice). This method proved extremely efficient, with a per site updating time of 160 ns. The heat-bath algorithm¹¹ was chosen to update individual spins, since it provides rapid thermalization in systems where there are a small number of states at each site. The system was a two-dimensional, 48x172 lattice with periodic boundary conditions. For the dynamic study, after initialization (either in a randomized “hot” configuration, or one of the “cold” $T=0$ ground states of the system), the lattice was allowed to relax for 50 000 passes in order to come to equilibrium at a desired temperature.

In the measurement portion of the run, row magnetizations $M(x,t)$ (the average spin in a row perpendicular to the axial direction) and the local energies of a representative group of sites were sampled every 100 Monte Carlo passes through the lattice. A current table of 100 such passes was maintained in order to compute, and then average, the temporal correlation functions of the local energies, as well as the spatial-temporal correlation function of the row magnetizations. A total of 50 000 measurement passes were taken, i.e., averages were taken over 500 configurations.

The linear response function

$$S(k, \omega) = \sum_{r,t} \exp[-i(kr - \omega t)] G(r, \tau) \quad (3)$$

which is the Fourier transform of the connected correlation function

$$G(r, \tau) = \sum_{x,t} [M(x+r, t+\tau)M(x,t) - \sum_{x,t} [M(x+r, t+\tau)] \sum_{x,t} [M(x,t)]] \quad (4)$$

exhibits a sharp peak at nonzero frequency and wave vector, but *only* within the incommensurate phase (Fig. 3). $M(x,t)$ is the time history of the row magnetizations. In the commensurate phase a weak peak is found at zero frequency, while the paramagnetic phase shows a broad, less intense peak. In order to confirm this behavior, we also looked at the axial next-nearest-neighbor Ising model, where the phase diagram is well established.¹²⁻¹⁵ The same behavior was observed: The sharp peak at nonzero frequency was *unique* to the incommensurate phase. The temperature dependence of the peak’s frequency, as well as the maximum intensity of the structure factor, are given in Fig. 4. The peak frequency increases monotonically with temperature within the incommensurate phase; the temperature where it first deviates from zero frequency is consistent with

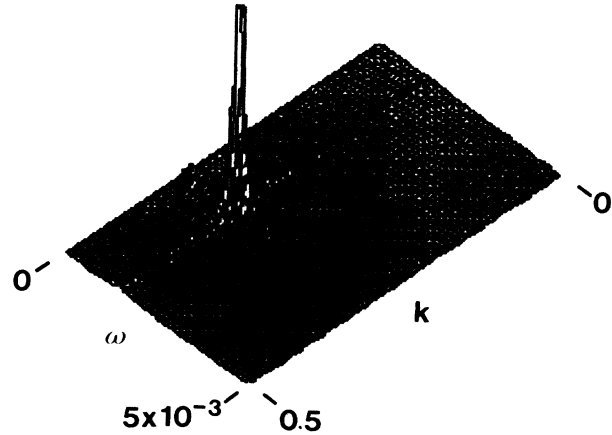


FIG. 3. $S(k, \omega)$ for $J_0 = +1, J_1 = -1, J_2 = -0.6, J_3 = +0.1, T = 1.4$.

the incommensurate-commensurate phase transition, as determined by the structure factor data.

The cause of this peak is found by examining row magnetization histories of the system. In the incommensurate phase (Fig. 5) the pattern is clearly propagating, with a velocity of 3.7×10^{-3} sites/pass. This drift of the incommensurate pattern has been previously observed by Selke and Fisher.⁷ The commensurate pattern [Fig. 5(c)] is locked to the lattice (note the fluctuation in position of a domain wall). In the paramagnetic phase [Fig. 5(a)] fluctuations have destroyed any long-range ordering, in space or time. Since an incommensurate pattern has no preferred location on the lattice, it should respond much more readily than a commensurate pattern to a driving force having an axial component. The four-color parquette parallel-updating scheme effectively provides such a force; since updating is performed sequentially along (1,1), disturbances will propagate in that direction. This anisotropic updating entrains the incommensurate pattern. Increased temperature loosens the pattern and increases the system response to this force.

The Fourier transform of the local-energy correlation shows two features: a constant background, corresponding to short-term fluctuations, and a peak due to pattern drift.

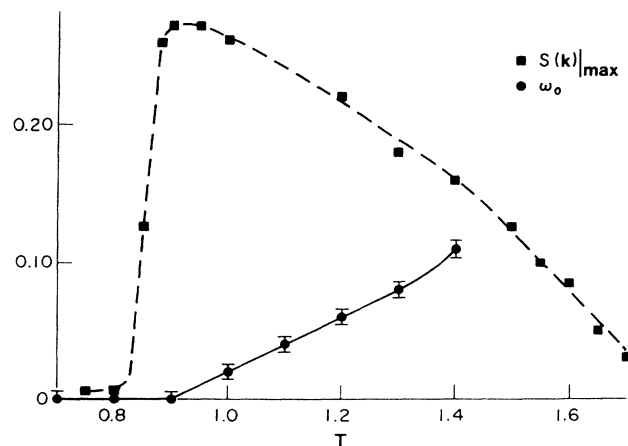


FIG. 4. Temperature dependence of ω_0 and $S(k)|_{max}$. Arbitrary units for $S(k)|_{max}$. All parameters as in Fig. 3, except T varies.

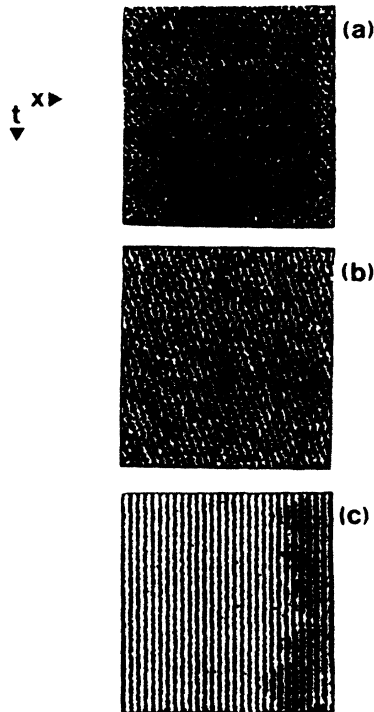


FIG. 5. Row-magnetization histories: (a) "paramagnetic" phase ($T=1.6$), (b) incommensurate phase ($T=1.4$), and (c) commensurate phase ($T=0.6$). All parameters as in Fig. 3, except T , as noted. Shading indicates row magnetization: pure white is $M=+1$, pure black is $M=-1$. Scale in the x direction is 86 lattice sites, in the t direction 10^5 lattice updates.

The central frequency of this peak is just twice that of $S(k, \omega)$, since equivalent energy fluctuations occur twice in the passage of a row-magnetization wave over a given lattice site. At the transition to the incommensurate phase, the kink diffusivity can be obtained from the width of the peak in $S(k, \omega)$, and the thermal diffusivity from the width of the Fourier-transformed energy correlation, using the fluctuation-dissipation theorem.

The fact that the kink diffusivity obtained from the present two-dimensional calculation is slightly larger than the thermal diffusivity is interesting when compared with earlier theoretical and experimental studies. In two different three-dimensional incommensurate insulators an unexpected high-speed diffusion has been observed. In BaMnF_4 , Lyons *et al.*¹⁶ find from the linewidths and k^2 dependence of dynamic central-mode scattering a diffusivity 20 times greater than the directly measured thermal diffusion constant in the same specimens.¹⁷ Similarly, in $\text{Ba}_2\text{NaNb}_5\text{O}_{15}$ Young and Scott¹⁸ infer a kink diffusivity

TABLE I. Diffusivity measurements.

	Theoretical		Experimental	
	1D SG-MD	2D Present	Quasi-2D BaMnF_4	3D $\text{BaNaNb}_5\text{O}_{15}$
D_k (cm^2/s)	0	...	0.14	1.3 ± 0.2
D_t (cm^2/s)	> 0	...	0.007	0.02
D_k/D_t	0	2 ± 0.5	20	65

which is 65 times as fast as that which can be calculated from the data of Burkhart and Rice.¹⁹ The diffusivity inferred by Young and Scott is manifested as an inverse relaxation time for acoustic phonons which varies as k^2 . It is important to note that $D_k=1$ cm^2/s observed in $\text{Ba}_2\text{NaNb}_5\text{O}_{15}$ and 0.14 cm^2/s in BaMnF_4 are about 10^3 times too fast to be due to ionic diffusion (e.g., of Na^+ ions in $\text{Ba}_2\text{NaNb}_5\text{O}_{15}$); such ionic diffusivities are of the order 10^{-4} cm^2 .²⁰⁻²² Thus, in two different structurally incommensurate insulators, two independent groups using unrelated experimental techniques have concluded that there is a diffusion one to two orders of magnitude faster than thermal diffusion of entropy fluctuations. Kink diffusion has been suggested as a possible explanation of the fast diffusive mode.²³

By comparison, molecular-dynamics model calculations²⁴ for the one-dimensional (1D) sine-Gordon model (SG-MD)¹ predict subdiffusive behavior for kinks ($\langle [r(t) - r(0)]^2 \rangle \propto t^{2/3}$, where r is the kink position). This gives a vanishing diffusion constant for kinks. The ordinary thermal diffusion (due to phonons) is nonzero, since the scattering rate for phonons in the model is finite. Therefore, the ratio $D_k/D_t=0$ for this 1D model. (The phonon-scattering rate goes to zero in the continuum limit, where the kink width is much larger than the lattice spacing. In that case the thermal diffusion constant must diverge.)

The present dynamical Monte Carlo study thus suggests (Table I) a bridge between previous 1D theoretical predictions and 3D experimental observations of kink and thermal diffusion.

In conclusion, the linear response function $S(k, \omega)$ appears to be a strong predictor of phases and phase transitions in incommensurate systems. It remains to check if this behavior is also manifested in Monte Carlo studies of other incommensurate systems, and if random-site updating destroys it, as the entrainment picture would suggest.

Discussions with Tom deGrand and Harry Jordan are gratefully acknowledged.

¹P. Bak, Rep. Prog. Phys. **45**, 587 (1982).

²J. Villain and P. Bak, J. Phys. (Paris) **42**, 657 (1981).

³R. M. Hornreich, R. Leibmann, H. G. Schuster, and W. Selke, Z. Phys. B **35**, 91 (1979).

⁴P. M. Duxbury and M. Barber, J. Phys. A **15**, 3219 (1982).

⁵M. Barber and W. Selke, J. Phys. A **15**, L617 (1982).

⁶M. E. Fisher and W. Selke, Phys. Rev. Lett. **44**, 1502 (1980).

⁷W. Selke and M. E. Fisher, Phys. Rev. B **20**, 257 (1979).

⁸Y. Yamada and N. Hamaya, J. Phys. Soc. Jpn. **52**, 3466 (1983).

⁹W. Selke, M. Baretto, and J. Yeomans (unpublished).

¹⁰W. Oed, Appl. Inf. **24**, 358 (1982).

¹¹M. Creutz, Phys. Rev. D **21**, 1006 (1980).

- ¹²W. Selke and J. Yeomans, *Z. Phys. B* **42**, 311 (1982).
¹³W. Selke, *Z. Phys. B* **42**, 335 (1982).
¹⁴P. Beale, P. Duxbury, and J. Yeomans, *Phys. Rev. B* **31**, 7166 (1985).
¹⁵P. Duxbury and M. Barber, *J. Phys. A* **15**, 3219 (1982).
¹⁶K. B. Lyons, R. N. Bhatt, T. J. Negran, and H. J. Guggenheim, *Phys. Rev. B* **25**, 1791 (1982).
¹⁷T. J. Negran, *Ferroelectrics* **34**, 31 (1981).
¹⁸P. W. Young and J. F. Scott, *Ferroelectrics* **52**, 35 (1983).
¹⁹G. H. Burkhardt and R. R. Rice, *J. Appl. Phys.* **48**, 4817 (1977).
²⁰K. Funke, *Prog. Solid State Chem.* **11**, 345 (1976).
²¹S. J. Allen, Jr. *et al.*, in *Superionic Conductors*, edited by G. D. Mahan and W. L. Roth (Plenum, New York, 1976), p. 279.
²²F. Habbal, J. Zvirgzds, and J. F. Scott, *J. Chem. Phys.* **69**, 4984 (1978).
²³D. W. Bechtle, J. F. Scott, and D. J. Lockwood, *Phys. Rev. B* **18**, 6213 (1978).
²⁴T. Schneider and E. Stoll, *Phys. Rev. B* **23**, 5317 (1980).

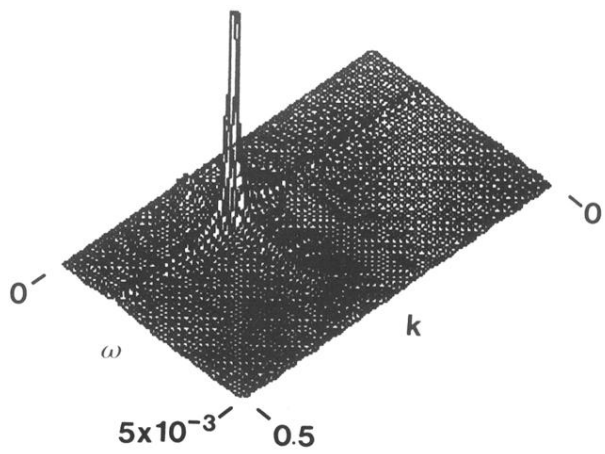


FIG. 3. $S(k, \omega)$ for $J_0 = +1$, $J_1 = -1$, $J_2 = -0.6$, $J_3 = +0.1$, $T = 1.4$.

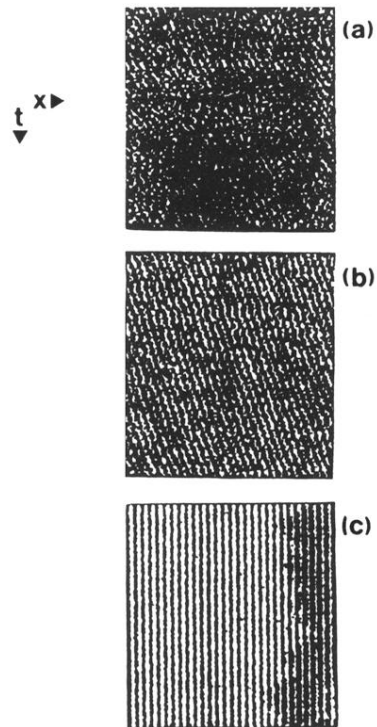


FIG. 5. Row-magnetization histories: (a) “paramagnetic” phase ($T = 1.6$), (b) incommensurate phase ($T = 1.4$), and (c) commensurate phase ($T = 0.6$). All parameters as in Fig. 3, except T , as noted. Shading indicates row magnetization: pure white is $M = +1$, pure black is $M = -1$. Scale in the x direction is 86 lattice sites, in the t direction 10^5 lattice updates.